

## Acoustic Separation of Moving Fibers in a Pulp Flow

J.H. Jong, M.H. Choi, J.P. Gerhardstein and P.H. Brodeur

Institute of Paper Science and Technology  
500 10th St. NW, Atlanta, GA, 30318 USA

### ABSTRACT

The use of an acoustic force to deflect moving wood pulp fibers in a pipe flow and, hence, separate fibers from water, was investigated. The goal is to devise a continuous process to increase the consistency of a pulp stream (pulp thickening). Experiments were performed using a prototype ultrasonic separation system capable of processing fiber suspensions at consistencies up to 2% and flow rates up to 180 L/min. In this setup, ultrasonic transducers mounted on one of the walls of a rectangular cross-section pipe are used to apply an acoustic force normal to the flow direction. Fibers deflect toward the opposite side wall as they interact with the ultrasonic field. At least three nonlinear effects are responsible for the acoustic force: acoustic radiation pressure, acoustic streaming, and acoustic cavitation. A CDD camera was used to record the deflection effect as a function of pulp consistency, flow velocity, transducer frequency, and acoustic intensity. Observations using softwood fibers show that as the acoustic intensity increases at constant flow velocity, the level of fiber deflection increases. On the other hand, higher flow velocity at constant acoustic intensity level decreases the deflection effect. Also critical is the change of pulp consistency as the attenuation of ultrasound increases with higher consistency pulp. Results were used to establish a preliminary analytical model to predict fiber deflection.

### INTRODUCTION

The study of wood pulp fiber suspensions interacting with an ultrasonic wave field has been an on-going research activity during the past decade [1-8]. In principle, when pulp fibers suspended in water are exposed to an ultrasonic wave field, they are subjected to a noncontact acoustic radiation force that results in the migration of fibers. Also, since fibers are nonspherical particles, they can reorient due to the presence of an acoustic radiation torque. In addition to acoustic radiation pressure, acoustic streaming and acoustic cavitation can contribute to the acoustic force. Altogether, these nonlinear acoustic effects are important because they enable the noncontact mechanical manipulation of fibers and other particles. Several applications have been explored. For example, an acoustic force has been used to compact a wet fiber mat in a small enclosure [5]. Observations showed that the degree of pulp compaction correlates to the degree of refining [5]. In a different application, the ultrasonic redistribution of vessel elements in hardwood pulp based on fiber width and projected area was studied [6]. Ultrasonic whitewater clarification in which chemical flocculation is used in combination with an ultrasonic field to clarify a whitewater stream was also recently investigated [8].

Another application, which is the focus of the work reported here, considers the use of a traveling ultrasonic wave field to deflect a pulp stream. The idea is to apply a normal force on flowing fibers for the purpose of increasing the consistency of the pulp stream. In other words, the desirable goal is to thicken a moving pulp suspension. Assuming that the characteristics of laminar and turbulent flow regimes exist in a moving pulp suspension at relatively low consistency up to 1 percent, the degree of fiber deflection varies as a function of consistency, flow velocity, acoustic frequency, and acoustic intensity (acoustic power per unit area). The effect of acoustic frequency is of particular importance because the contributing effects of acoustic radiation pressure, acoustic streaming, and acoustic cavitation are frequency dependent. The experimental setup to study fiber deflection is described next. Following this, results are reported and discussed. Finally, a preliminary analytical model of the fiber deflection mechanism is introduced.

### EXPERIMENTAL SETUP

To demonstrate the concept of separating fibers in a moving pulp suspension, a laboratory-scale flow-loop system available at IPST was used. Figure 1 shows a schematic diagram of the flow loop. Pulp stock at a given consistency is prepared in the 500-liter feed tank. A centrifugal pump is used to transfer the pulp to the bottom of a vertically

oriented acrylic pipe of rectangular cross-section. At the top of the pipe is an acoustic section consisting of transducers and absorbers opposing one another. Upon entering the acoustic section (magnified in the top right corner of the figure), fibers are deflected by a transverse acoustic force in such a way that two output streams can be obtained: one stream with highly deflected fibers on the absorber side (concentrated stream) and one stream with barely deflected fibers on the transducer side (diluted stream). By installing a mechanical divider blade above the in-line acoustic separator, deflected fibers can be separated and collected into the concentrated stream side. If all fibers are collected on the concentrated side, pulp thickening and/or dewatering is achieved. The position of the divider blade is adjustable.

The acoustic section consists of three pairs of 5- x 10-cm transducers and absorbers. The transducer-absorber separation distance is 15 cm. Function generators are used to supply continuous sine wave signals to broadband power amplifiers and impedance matching networks, which are used to amplify the signals and optimize electrical power transfer to the transducers, respectively. The setup is instrumented to allow measurements of several variables, including electrical power, acoustic intensity, and volume flow rate. A CCD camera is used to monitor pulp deflection in the acoustic section. The main interest in the investigation was to study pulp deflection under different conditions rather than optimizing separation using the divider blade.

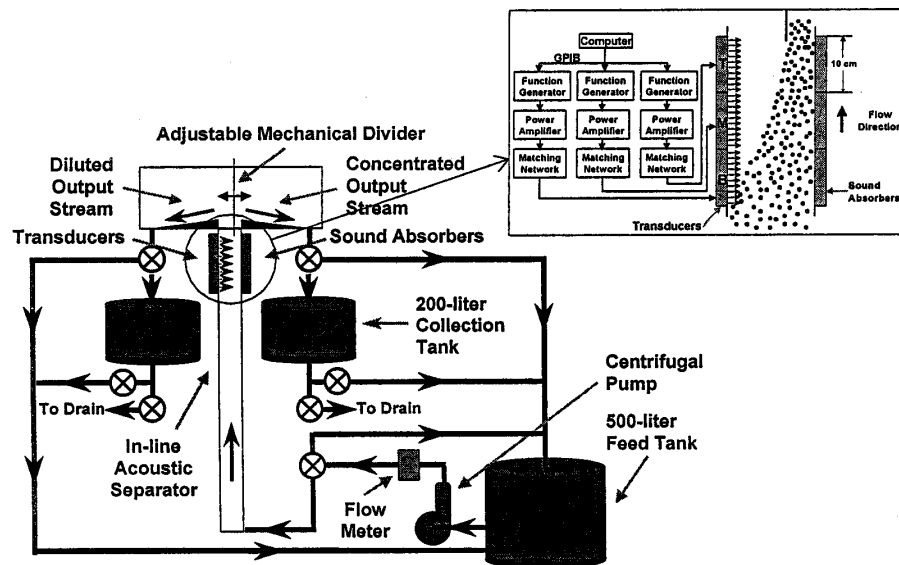


Figure 1. Schematic diagram of the experimental setup. A close-up of the in-line acoustic separator is shown in the top right corner of the figure.

All experiments were performed using never-dried softwood fibers. Softwood fibers were selected on the basis of larger fiber length and projected area when compared to hardwood fibers and, hence, larger acoustic force acting on the fibers. Table I provides a brief description of the softwood pulp. Observations were obtained at five different consistencies: 0.01%, 0.05%, 0.1%, 0.5%, and 1.0%. Also, transducers operating at three different frequencies were used: 60 kHz, 150 kHz, and 1.5 MHz.

Table I Softwood pulp properties: A Kajaani FS-100 analyzer was used to determine fiber parameters.

Furnish	Unbeaten Southern hard pine with less than 3% of hardwood
Arithmetic Fiber Length	$3.2 \pm 0.8$ mm
Arithmetic Fiber Width	$39.9 \pm 13.6$ $\mu$ m
Arithmetic Fiber Curl Index	$1.3 \pm 0.3$
CSF Number	740 ml

## EXPERIMENTAL RESULTS

Figure 2 represents a series of pulp deflection recordings using 150 kHz transducers at constant flow velocity (0.2 m/s) for different acoustic intensity levels. Transducers are located on the left-hand side of the photographs. Sound absorbers are located at the opposite side. Pulp consistency is 0.5%. It is observed that the deflection angles with respect to the vertical line along the transducers tend to increase as the acoustic intensity increases. At constant acoustic intensity, the deflection angle is significantly higher at 150 kHz than at 60 kHz. Additional recordings at 1.5 MHz (not shown) indicate that the deflection angles for this frequency are somewhat in-between results at 60 kHz and 150 kHz. This suggests that there is an optimum frequency for pulp deflection.

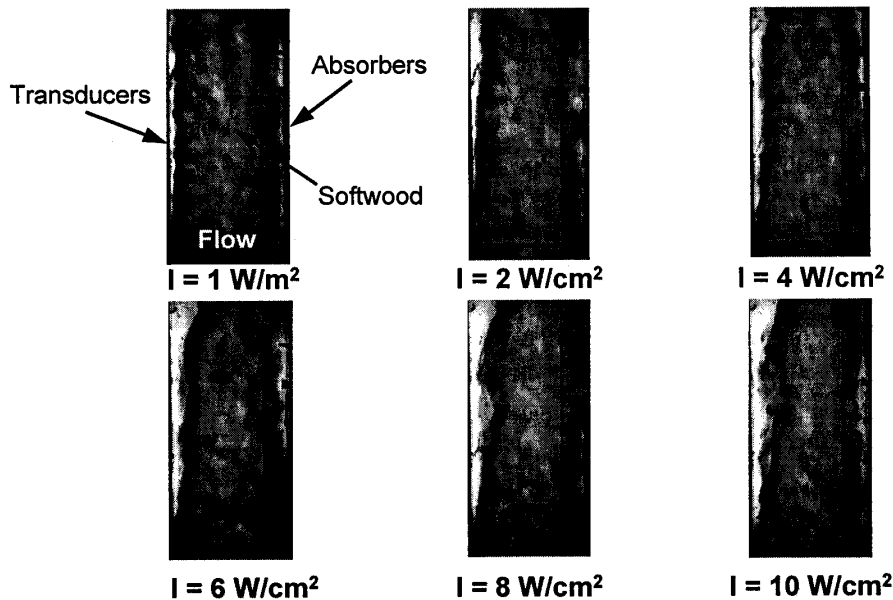


Figure 2. Deflection of moving softwood pulp for different acoustic intensities ( $f = 150$  kHz,  $v = 0.2$  m/s,  $C = 0.5$  %) White areas seen on the left-hand side of the photographs represent pure water.

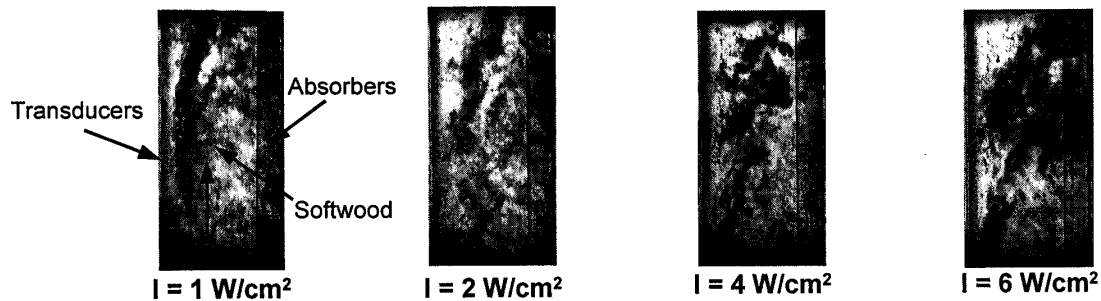


Figure 3. Deflection of moving softwood pulp for different acoustic intensities ( $f = 150$  kHz,  $v = 0.05$  m/s,  $C = 0.1$  %).

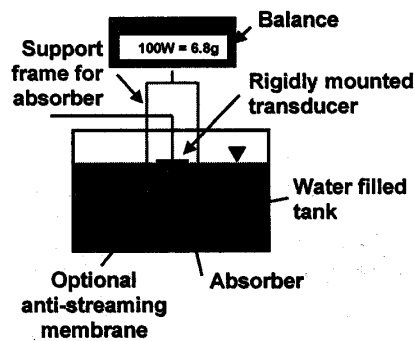
In Figure 3, photographs of deflection experiments are shown for consistency of 0.1%, flow velocity at 0.05 m/s, and 150-kHz transducer frequency. As the acoustic intensity increases, deflection angle increases but so does fluid-fiber interaction. As a matter of fact, several observations show that the deflection effect is more visible when the flow velocity is above 0.3 m/s.

Several complex observations have been made about the deflection effect:

- 1) A circulating backflow toward the transducer side is observed between transducers and absorbers due to the rectangular shape of the pipe and nonuniformity of the acoustic field. This circulating backflow decreases the overall efficiency of pulp deflection by deflecting back some fibers toward the transducers.
- 2) At the gap between two transducers, there is a phase mismatch creating a dead zone where no acoustic force is available (discontinuity).
- 3) Along the acrylic wall surfaces on either side of the transducers in perpendicular direction to the transducers, fibers tend to slow down due to no-slip boundary conditions, and backflow. This undesirable effect further contributes to reduce the overall efficiency of pulp deflection.
- 4) For lower consistency pulp (<0.1%), two deflection lines are observed, most likely due to (1) and (3). The primary deflection line further away from the transducers was given major attention since it was created by pure acoustic force without the resistances from the circulating backflow and/or the wall surface effect.

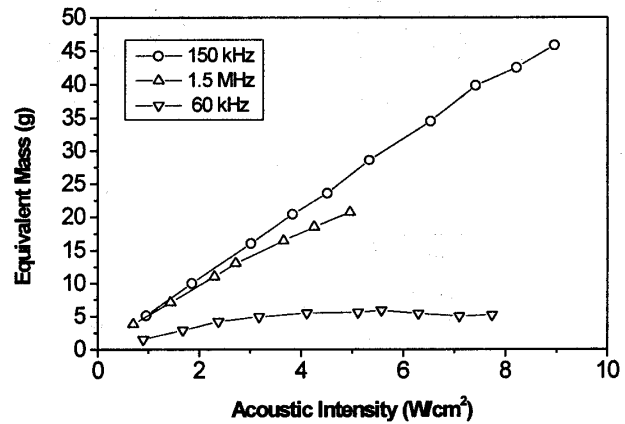
In short, there appears to be an optimal deflection condition available to get the maximum deflection efficiency. However, it is not trivial to estimate the optimal condition with only the preliminary set of results available. There are at least four important variables to consider for the estimation: consistency, flow velocity, acoustic frequency and acoustic intensity. It is likely that other cross-sectional pipe configurations need to be considered to reduce backflow and wall effects, including transducers with a concave surface to generate a focused ultrasonic field.

As briefly mentioned, three mechanisms may be responsible for the acoustic force. They are acoustic radiation pressure (ARP), acoustic streaming, and acoustic cavitation. The ARP-induced force is a steady time-averaged force acting on obstacles in the propagation path of an ultrasonic wave. It is a vector quantity as opposed to the conventional scalar hydrostatic pressure and is related to the change in the magnitude of the momentum carried by the wave at an obstacle [9]. Acoustic streaming is the flow motion caused by gradual absorption of the ultrasonic field by the liquid. Acoustic cavitation is the generation of bubbles when a liquid containing dissolved gas is subjected to an ultrasonic field [10,11]. As the bubbles form a jet stream, the surrounding liquid and fibers may be entrained and generate motions.



(a) Acoustic balancing equipment

Figure 4. Acoustic balancing measurements.



(b) Balancing results

In order to physically measure the acoustic force acting on fibers, a simple acoustic balancing test apparatus was built to convert the acoustic force to equivalent mass as shown in Figure 4 (a). Measurements are done in a small water tank at room temperature. A sound absorber submerged under water is supported by a metal frame attached to a balance located above the tank. An anti-streaming membrane was optionally designed to block streaming effect, but not used for the data in Figure 4(b). A test transducer was rigidly mounted above the absorber. A power meter connected to the transducer monitored the supplied electrical power. When the transducer was excited, the balance

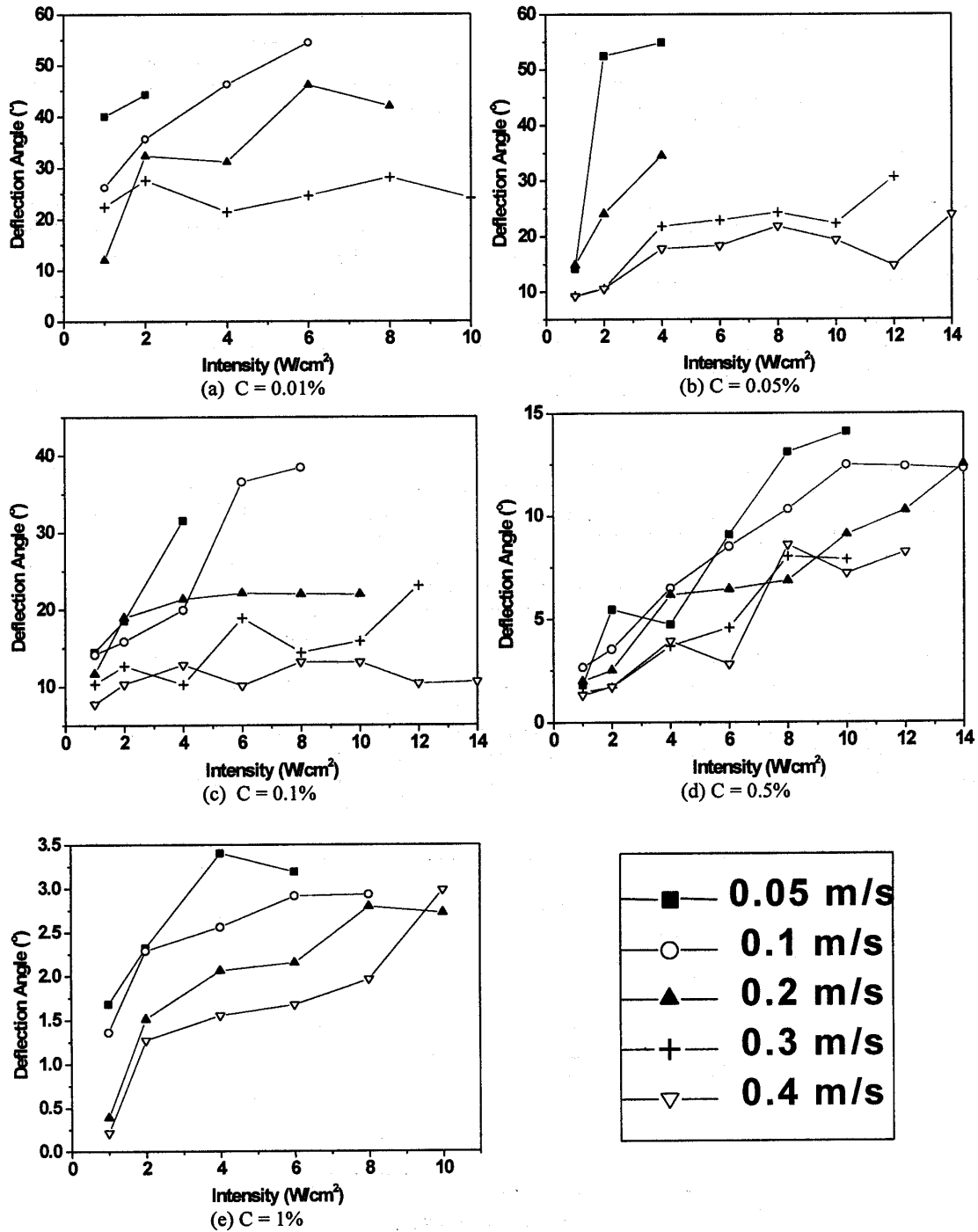


Figure 5. Comparison of deflection angles as a function of acoustic intensity and flow velocity for different consistency levels ( $f=150$  kHz).

recorded the corresponding equivalent mass due to the acoustic force. Results for measurements at 60 kHz, 150 kHz, and 1.5 MHz are plotted in Figure 4 (b). At 150 kHz, the equivalent mass seems to increase linearly with acoustic intensity. At 60 kHz, the equivalent mass first increases but quickly reaches a plateau at approximately 3 W/cm<sup>2</sup>. Adding more power has no significant effect on the equivalent mass. The start of the plateau may be considered as a cavitation threshold. Results at 1.5 MHz show an increase but appear to start leveling off at the maximum allowable intensity. No measurements above 5 W/cm<sup>2</sup> were taken at this frequency due to potential electrical arcing with the thin 1.5-MHz transducers.

The reason for the observed trends at different frequencies is not obvious, but the most likely explanation seems to be related to acoustic cavitation. At 1.5 MHz, very few bubbles are created and their size is very small due to the small acoustic wavelength ( $\lambda = 1$  mm). At 150 kHz, more bubbles and a bubble stream jet are visible and the bubble size is somewhat larger due to the larger wavelength ( $\lambda = 1$  cm). At 60 kHz, the amount of cavitation bubbles increases as the intensity increases and the bubble radius is larger than at the other frequencies. The wavelength in water is 2.5 cm at 60 kHz. Results at this frequency imply that too many bubbles decrease the acoustic force because the ultrasonic field is likely to be dissipated and attenuated by the large number of bubbles as well as large size bubbles. Therefore, there should be an optimal amount of cavitation bubbles as well as an optimal bubble size in order to generate maximum allowable acoustic force at a certain frequency. Further investigation is in progress with degassed water.

Figure 5 shows the combined results of the deflection angle in degrees as a function of acoustic intensity and flow velocity at 5 different consistencies (0.01%, 0.05%, 0.1%, 0.5%, and 1%). The transducer frequency is 150 kHz. Each deflection angle was measured at each test condition (5 measurements per data point). Because the deflection profile was somewhat unstable due to disturbances such as backflow, wall effects, and flow oscillation, each angle measurement was taken with caution. At the low consistency of 0.01%, the initial deflection angle can be as high as 45-55° but tends to level off at a certain acoustic intensity (approximately 6 W/cm<sup>2</sup>). This trend is repeatedly observed at other consistencies. In order to physically understand this behavior, a more relevant parameter needs to be used. To simplify the problem, one can assume that the initial deflection is linear, although realistically the deflection is likely to be curved due to inertia and changing resistance (see next section). Then, a vector relation can be used between the suspension flow velocity  $U_f$  and deflected velocity  $v$  with deflection angle  $\theta$ . The simple vector relation is  $v = U_f \tan \theta$ . Since one would expect that the deflected velocity normal to the flow direction,  $v$ , would remain constant under the same acoustic intensity and consistency, results in Figure 6 can be represented as a single curve independent of the flow velocity  $U_f$ . Then, the relationship between the deflected velocity  $v$  and acoustic intensity can be sought at a given consistency. Since Figure 5 (b) already show that the acoustic force tends to increase linearly with intensity at 150 kHz, the acoustic force can be related to the deflected velocity  $v$ .

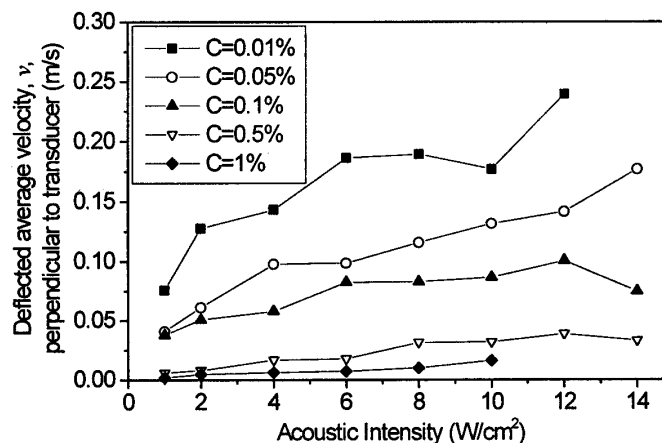


Figure 6. Average velocity of fiber deflection in the direction normal to the flow direction as a function of acoustic intensity for different consistency levels (0.01%, 0.05%, 0.1%, 0.5%, and 1%). Deflection angle data in Figure 6 were used in the calculations ( $f=150$  kHz).

Figure 6 shows the deflected average velocity  $v$  normal to the flow direction as the acoustic intensity increases. Results are based on converting deflection angle measurements to the deflected velocity using the data in Figure 5. The results at all consistencies tend to show a linear increase of the deflected velocity  $v$ . As expected, the lower the consistency is, the larger the deflected velocities are. This is due to the increasing resistance of the agglomerating fibers during the deflection process. At 1% consistency, the fiber mat becomes so dense that it would require more power than is available from our transducers to generate significant deflection.

### ANALYTICAL MODELING OF THE FIBER DEFLECTION EFFECT

In order to fundamentally understand the deflection behavior and estimate the deflection angle for a certain set of conditions (prediction), the development of an analytical model was undertaken to explain the mechanism. A physical representation of the actual deflection phenomenon is difficult. However, several assumptions can be made to simplify the deflection behavior. Let's consider two simple cases as shown in Figure 7: dilute region and dense region. In the "dilute region," one can assume that the suspension is sufficiently dilute so that it can be considered as a highly viscous liquid. This concept was introduced by Jong [12] for the compression of low-consistency fiber mats. Although it is currently not possible to define "dilute" in terms of consistency, we will tentatively consider 1% consistency as the maximum limit for the dilute case. This is based on the results in Figure 6, which can be interpreted as "Acoustic force is linearly proportional to deflected velocity up to 1% consistency." This is analogous to the force-damping mechanism and is further explored below.

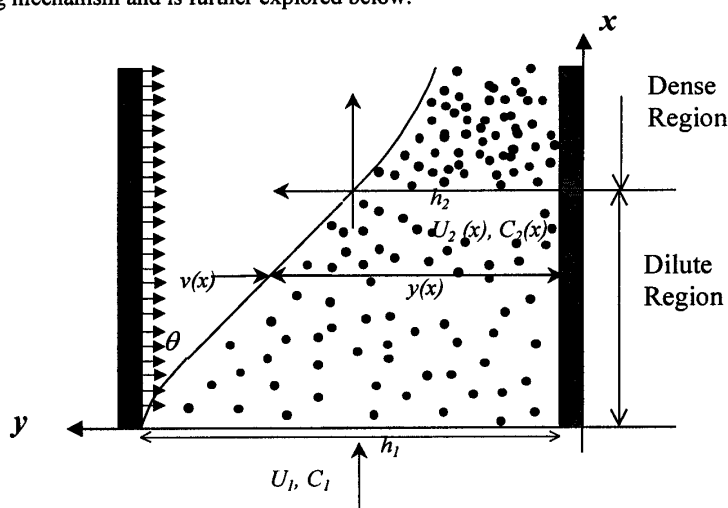


Figure 7. Representation of Deflection Regions

In the "dense region," as the fibers are further deflected/compressed at higher consistency, the fiber mat builds up enough resistance against the acoustic force. Therefore, the fiber can no longer be deflected linearly. This region is modeled by introducing Newton's 2nd law and Darcy's law to relate pressure balance to the governing equation along with continuity and conservation of fiber mass.

So far, the acoustic force is assumed to be constant for simplicity, although ARP, acoustic streaming, and cavitation are identified as part of this force. Further work is required in this area.

#### Case I Dilute Suspension

Introducing the concept similar to Jong [12], the governing equations for the case of a dilute suspension can be written as follows, assuming the resisting force varies linearly with velocity:

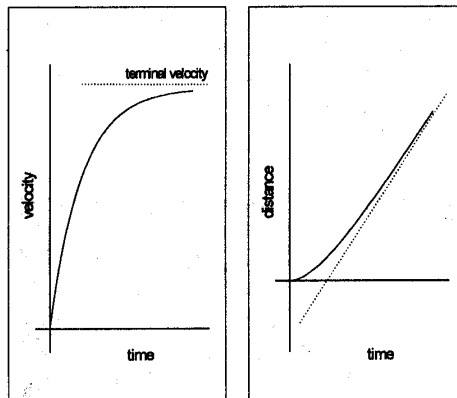
$$M_s \cdot \frac{d^2 y}{dt^2} + C_d \cdot \frac{dy}{dt} = F_{total} = M_{eq} \cdot g, \quad (1)$$

where  $M_s$  is the mass of the suspension,  $C_d$  is the damping coefficient, and  $F_{total}$  is the total acoustic force acting on suspension. Since the velocity  $v=dy/dt$ , the above differential equation can be simplified as a first-order differential equation. Solving it for  $v$  with the initial condition of  $v=0$  at  $t=0$  gives

$$\frac{dy}{dt} = v = \frac{F_{total}}{C_d} \left( 1 - \text{Exp} \left[ -\frac{C_d}{M_s} \cdot t \right] \right) \quad (2)$$

Integrating Eq. 2 to find  $y$  with the initial condition of  $y=0$  at  $t=0$ , it can be solved for  $y$  as a function of  $t$ :

$$y = \frac{F_{total}}{C_d} \left( t + \frac{M_s}{C_d} \text{Exp} \left[ -\frac{C_d}{M_s} \cdot t \right] \right) - \frac{F_{total} \cdot M_s}{C_d^2} \quad (3)$$



(a) Velocity vs. time (b) Distance vs. time

Figure 8. Predicted velocity and distance curves of fibers as a function of time in a highly viscous liquid.

Since  $F_{total}$  is a constant acoustic force applied instantaneously to the suspension as a step function when  $t=0$ , the velocity and the distance traveled by the deflection with respect to time are shown in Figure 8. The deflection quickly reaches a terminal velocity  $v_t$  depending on  $F_{total}$  and  $C_d$  as follows:

$$v_t = \frac{F_{total}}{C_d} \quad (4)$$

The damping coefficient  $C_d$  can be estimated either from data in Figure 6 or independently from a simple experiment at the required consistency.

### Case II Dense Region

In order to model the pulp deflection in the dense region, the following approach is taken in a manner similar to the concept developed by Jong [12]. Referring to Figure 7, the flow velocity  $U_1$  is effectively constant with  $x$ , i.e.,  $U_1=U_2(x)$ . This is reasonable due to constant area. It is assumed that the motion along the  $y$  axis is thus convected at the speed  $U_2(x)$ . Hence, it is identical to the motion of a cylinder of length  $y(x)$  that impinges on a solid boundary at rest as shown in Figure 9. As the cylinder impinges, the same magnitude of reaction occurs. As  $y(x)$  decreases with the speed of  $v(x)$ , the water present in the cylinder is removed at the speed of  $v(x)$ . The time since impact is  $t=x/U_2(x)$ .

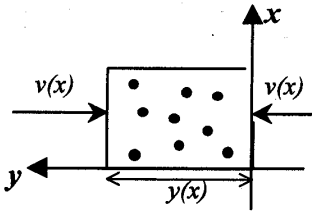


Figure 9. Motion of a cylinder.

A simple application of Newton's second law in the  $x$  direction defines the pressure distribution at the surface of the deflected mat, i.e.,

$$\frac{d\{\rho_1 \cdot v(x) \cdot y(x)\}}{dt} = -\rho_2 \cdot \mu \cdot SFR \cdot y(x) \cdot C_2(x) \cdot v(x), \quad (5)$$

where  $\mu$  is the dynamic viscosity ((N·s)/m<sup>2</sup>) and  $SFR$  is the Specific Filtration Resistance (m/kg) of the mat. The right-hand side is a modified Darcy's law that predicts the pressure difference based on fluid and fiber properties. The derivation of the modified form is briefly introduced in Appendix A. Also, by assuming that the densities and  $\rho_2$  are equal, the equation can be further simplified for convenience. Continuity gives,

$$\frac{d}{dt} \{y(x)\} = -v(x). \quad (6)$$

By assuming that all fibers are deflected, the conservation of fibers at a given location is written as

$$h \cdot C_1 = y(x) \cdot C_2(x), \quad (7)$$

where  $h$  is the cell height (m). Eqs. 5, 6, and 7 can be analytically or numerically solved to predict the deflection curve  $y(x)$ . Appendix B shows the analytical solution of the above governing equations. One of the difficult parts is to estimate the mat resistance  $SFR$ . It is expected that  $SFR$  varies as the fibers are deflected due to consistency change. Further work is required on this issue.

## CONCLUSIONS

This study has shown that the concept of separating softwood fibers from water in a pipe flow using an ultrasonic wave field is feasible and industrial applications can be envisioned. Three nonlinear acoustic effects are responsible for the acoustic force applied on the fibers: acoustic radiation pressure, acoustic streaming, and acoustic cavitation. Observations show that as the acoustic intensity increases at constant flow velocity, the level of fiber deflection increases. On the other hand, higher flow velocity at constant acoustic intensity decreases the deflection effect. As expected, fiber deflection decreases as pulp consistency increases. Visual observations and acoustic balancing measurements indicate that an optimal frequency exists. Even though the best results were obtained at 150 kHz in this work, this frequency is by no means optimal. A preliminary form of an analytical model was proposed to predict the fiber deflection curve in dilute and dense regions. The model assumes that a dilute fiber suspension can be considered as a highly viscous liquid while in a dense suspension, and, hence, fibers are subjected to compression according to Newton's 2<sup>nd</sup> law and Darcy's law. The specific filtration resistance of the mat, however, is unknown at this time.

## ACKNOWLEDGEMENTS

The authors would like to thank the collaboration of F. Bose and D. Silimon from IPST for the setup of experiments and the valuable comments by D. Grimes and J. Milliken from Beloit Corporation. The authors would also like to acknowledge the support of the Member Companies of the Institute of Paper Science and Technology, the U.S.

Department of Energy, Office of Industrial Technologies through its Agenda 2020 Program for the Pulp and Paper Industry (Cooperative Agreement #DE-FC07-97ID13553), and the State of Georgia through its Traditional Industry Program in Pulp and Paper (TIP<sup>3</sup>).

## REFERENCES

1. Brodeur, P.H., Dion, J.L., Garceau, J.J., Pelletier, G., and Massicotte, D., "Fiber Characterization in a Stationary Ultrasonic Field," *IEEE Trans. Ultrason. Ferroelec. Freq. Control.* 36:549-553 (1989).
2. Garceau, J.J., Dion, J.L., Brodeur, P., and Luo, H., "Acousto-optical Fiber Characterization," *Tappi J.* 72:171-173 (1989).
3. Brodeur, P.H., "Motion of Fluid Suspended Fibers in a Standing Wave Field," *Ultrasonics* 29:302-307 (1991).
4. Brodeur, P.H., "Acoustic Separation in a Laminar Flow," *Proc. IEEE Ultrasonics Symp., Cannes, France Vol. 3:1359-1362* (1994).
5. Brodeur, P.H. and Runge, T.M., "Compactibility of a Wet Fiber Mat Using Acoustic Radiation Pressure," *J.Pulp Paper Sci.* 22(8): J278-J282 (1996).
6. Oakland, M.O., "Separation of Vessel Elements from Hardwood Fibers Using an Ultrasonic Method," *M.S. Research Report, IPST* (1997).
7. Brodeur, P.H., "Method and Apparatus for Acoustic Fiber Fractionation," *U.S. Patent #5,803,270*, Sept. 8, (1998).
8. Brodeur, P.H., Deng, Y., Gerhardstein, J.P., Bose, F., and Yan Z., "Whitewater Clarification using a Dual Flocculation/Ultrasonic Method," submitted to *J. Pulp & Paper Sci.* (1999).
9. Shutilov, V.A., "Fundamental Physics of Ultrasound," *Gordon and Breach Sciences Publishers, QC244.S4723* (1988).
10. Neppiras, "Acoustic Cavitation," *Phys. Rep.*, 61, 159-251 (1980).
11. Blanz, J., "The Application of Acoustic Cavitation Towards Refining of Cellulose Fibers," *M.S. Research Report, IPST* (1997).
12. Jong, J.H., "Characteristics of Jet Impingement, Drainage and Compression in a Forming Roll of a Twin-Wire Machine," *Ph.D. Thesis, University of Toronto* (1998)

## APPENDIX A

The governing equations describing flow through a fiber mat can be derived from Darcy's law, which was originally developed from experiments on water flow through a bed of uniform sand. Darcy's law states that "the rate of flow (volume per unit time)  $Q$  is proportional to the constant cross-sectional area  $A$  and is also proportional to the piezometric head  $\Delta P$  and inversely proportional to the height of a porous medium  $h$ ." It can be formulated as

$$v = \frac{Q}{A} = \frac{K \Delta P}{\mu h}, \quad (\text{A-1})$$

where  $v$  is the average flow velocity (m/s),  $Q$  is the volume flow rate (m<sup>3</sup>/s),  $A$  is the cross-sectional area of the porous medium (m<sup>2</sup>),  $h$  is the height of the porous media (m),  $\Delta P$  is pressure drop (Pa), and  $K$  is the permeability (m<sup>2</sup>) of the porous matrix, which is solely dependent on properties of the solid matrix. The dynamic viscosity  $\mu$  ((N·s)/m<sup>2</sup>) is the only fluid property in the formula. For a fiber mat, the mat height  $h$  is equal to the basis weight  $BW$ , divided by the mass concentration  $c_m$ . Hence,

$$\Delta P = \frac{\mu}{K} \cdot v \cdot \frac{BW}{c_m}, \quad (\text{A-2})$$

where  $BW$  has units of kg/m<sup>2</sup> and  $c_m$  has units of kg/m<sup>3</sup>. Here,  $K$  and  $c_m$  are determined by the properties of the fiber mat for a constant  $BW$ . The term  $1/(K \cdot c_m)$ , which combines them, is typically referred to as the Specific Filtration Resistance (*SFR*).

$$\Delta P = \mu \cdot \left( \frac{1}{K \cdot c_m} \right) \cdot v \cdot BW = \mu \cdot SFR \cdot v \cdot BW = \mu \cdot SFR \cdot v \cdot \rho \cdot C \cdot y, \quad (A-3)$$

where the *SFR* has units of m/kg,  $\rho$  is the wet mat density,  $y$  is the mat height, and  $C$  is the consistency.

## APPENDIX B

The governing equations are given in Eqs. 5, 6, and 7.

Since  $dx = U_1 \cdot dt$ , Eq. 5 becomes

$$\frac{d\{\rho_1 \cdot v(x) \cdot y(x)\}}{dx/U_1} = -\rho_2 \cdot \mu \cdot SFR \cdot y(x) \cdot C_2(x) \cdot v(x). \quad (A-4)$$

Assume  $\rho_1 = \rho_2$  and differentiate the above equation along with Eq. 7,

$$U_1 \left( v(x) \cdot \frac{dy(x)}{dx} + y(x) \cdot \frac{dv(x)}{dx} \right) = -\mu \cdot SFR \cdot h \cdot C_1 \cdot v(x). \quad (A-5)$$

By using Eq. 6, its differentiation with respect to  $x$ , and expressing the equation in terms of  $y(x)$ ,  $y'(x)$  and  $y''(x)$ ,

$$U_1 \left( y(x) \cdot \left( -U_1 \cdot \frac{d^2 y(x)}{dx^2} \right) \right) = U_1^2 \cdot \left( \frac{dy(x)}{dx} \right)^2 - \mu \cdot SFR \cdot y(x) \cdot C_2(x) \cdot \left( -U_1 \cdot \frac{dy(x)}{dx} \right) - U_1^2 \cdot y \cdot y'' = U_1^2 \cdot (y')^2 + \mu \cdot SFR \cdot h \cdot C_1 \cdot U_1 \cdot y'.$$

Then,

$$y \cdot y'' = -(y')^2 - \frac{\mu \cdot SFR \cdot h \cdot C_1}{U_1} \cdot y'. \quad (A-6)$$

Let  $\frac{\mu \cdot SFR \cdot h \cdot C_1}{U_1} = K_1$ .

Also, boundary equations are: i) at  $x=0$ ,  $y(0)=h$ , and ii) at  $x=0$ ,  $y'(0)=-v(0)/U_1=-\tan\theta$ .

Let  $P = dy(x)/dx = y'$ . Then,  $dP/dx = y'' = dP/dy \cdot dy/dx = P' \cdot P$ . Therefore, Eq. A-6 can be written as

$$y \cdot P' \cdot P = -P^2 - K_1 \cdot P$$

$$\frac{dP}{P + K_1} = -\frac{dy}{y} \quad (A-7)$$

Integrate and find the integration constant  $K_2$ , the resulting equation becomes

$$y' = \frac{K_2}{y} - K_1, \quad (A-8)$$

where  $K_2 = h \cdot (K_1 - \tan\theta)$ . By integrating Eq. A-8, the final relationship becomes,

$$\frac{h-y}{K_1} + \frac{K_2}{K_1^2} \cdot \ln \frac{K_2 - K_1 \cdot h}{K_2 - K_1 \cdot y} = x. \quad (A-9)$$